Environmental Science & Technology

pubs.acs.org/est

Article

Improvements to the Accuracy of Atmospheric Oxidized Mercury Measurements

Seth N. Lyman,* Lynne E. Gratz, Sarrah M. Dunham-Cheatham, Mae Sexauer Gustin, and Adriel Luippold

Cite This: *Environ. Sci. Technol.* 2020, 54, 13379−13388

Read Online

ACCESS | Metrics & More | Article Recommendations | Supporting Information

ABSTRACT: We developed a cation-exchange membrane-based dual-channel system to measure elemental and oxidized mercury and deployed it with an automated calibration system and the University of Nevada, Reno-Reactive Mercury Active System (UNR-RMAS) at a rural/suburban field site in Colorado during the summer of 2018. Unlike oxidized mercury measurements collected via the widely used KCl denuder method, the dual-channel system was able to quantitatively recover $HgCl_2$ and $HgBr_2$ injected by the calibrator into the ambient sample air and compared well with the UNR-RMAS measurements. The system measured at 10 min intervals and had a 3-h average detection limit for oxidized mercury of 33 pg m^{-3}. It was able to detect day-to-day variability and diel cycles in oxidized mercury (0 to 200 pg m^{-3}) and will be an important tool for future studies of atmospheric mercury. We used a gravimetric method to independently determine the total mercury permeation rate from the permeation tubes. Permeation rates derived from the gravimetric method matched the permeation rates observed via mercury measurement devices to within 25% when the mercury permeation rate was relatively high (up to 30 pg s^{-1}), but the agreement decreased for lower permeation rates, probably because of increased uncertainty in the gravimetric measurements.

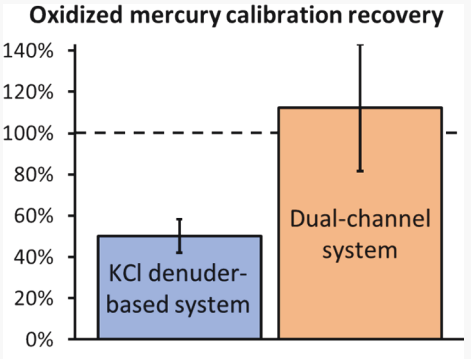

KEYWORDS: *permeation tube, oxidized mercury, mercury calibrator, dual-channel, UNR-RMAS*

1. INTRODUCTION

Mercury is a pervasive environmental contaminant that impacts the health of humans and wildlife.[1−4] Most mercury pollution is emitted to the atmosphere, but its toxic impact generally occurs after it deposits into ecosystems.[5] Atmospheric transport and chemistry determine where and when these toxic impacts occur.[5−7]

A critical aspect of atmospheric mercury behavior is the oxidation of elemental mercury (Hg^0). The majority of mercury is emitted as Hg^0,[8] which is relatively inert and can be transported around the globe.[9] However, Hg^0 can be oxidized in the atmosphere,[10−14] forming oxidized mercury compounds that are much more reactive, water-soluble, and readily depositable.[6] In this work, we refer to oxidized mercury as Hg^{II} because mercury in the +1 oxidation state is very likely rare in the natural environment.[15,16] Low concentrations and the reactivity of Hg^{II} makes it impossible for existing methods to quantitatively differentiate between gas and particle phase Hg^{II}.[17,18]

Recent theoretical work has pointed to halogen radicals (especially bromine) as important initiators of Hg^0 oxidation reactions.[19−21] Still, some have argued that models can only explain measured Hg^{II} behavior if they include reactions with other oxidants, including ozone and OH radical.[13,22−24] The actual chemical speciation of atmospheric Hg^{II} is not known with certainty, since no successful compound-specific measurements have been made in ambient air.[25−27] A wide range of compounds have been proposed.[6,19,20,24,28−35] The University of Nevada, Reno-Reactive Mercury Active System (UNR-RMAS) collects Hg^{II} on nylon membranes, and the collected Hg^{II} can be thermally desorbed into a mercury analyzer. By comparing the thermal desorption profiles of synthetic standards against those of ambient air samples, researchers have found consistent evidence for Hg^{II} compounds containing halogens, nitrogen, oxygen, and sulfur.[36,37] UNR-RMAS results have been shown to be consistent with known atmospheric chemistry and transport at sites around the globe.[28,29,38]

Work to understand mercury oxidation and reduction in the ambient atmosphere has been confounded by inaccuracy in commercial Hg^{II} measurement systems.[17,39−41] These systems rely on KCl-coated denuders to capture Hg^{II} compounds, but a substantial amount of the Hg^{II} they capture is reduced to Hg^0 during sample collection, causing a low bias for Hg^{II}.[42] Because

Received: April 30, 2020
Revised: August 20, 2020
Accepted: October 12, 2020
Published: October 19, 2020

https://dx.doi.org/10.1021/acs.est.0c02747
Environ. Sci. Technol. 2020, 54, 13379−13388

the extent of the bias depends on ambient conditions and the Hg^{II} compounds being measured,[39,43] correcting for the bias in existing data sets may not be possible. This bias has left modelers without reliable Hg^{II} data sets to compare against model outputs, making it difficult to answer questions about mercury oxidation mechanisms.

The bias in KCl denuder-based Hg^{II} measurements was discovered about a decade after the technique had begun to be widely used.[42,44] At least part of the reason for this delay was that, until recently, no technique existed to routinely check the accuracy of Hg^{II} measurements in ambient air.[45] Permeation tube[43,46] and evaporation[47] methods have now been used to calibrate for Hg^{II} compounds at ambient or near-ambient levels.

Several recent papers, including papers that incorporate Hg^{II} calibrations, have shown that activated poly(ether sulfone) cation-exchange membranes collect Hg^{II} compounds without the bias inherent in KCl denuder-based methods.[36,37,43,48] Unfortunately, while the preconcentration time required for KCl denuder measurements is usually only 1 h, direct collection of Hg^{II} on cation-exchange membranes requires long sampling times (generally at least 1 week).[28] While accuracy is more important than sampling frequency, an accurate, high-frequency measurement system is also needed.

Here we report on the development of a mercury measurement system that switches between a cation-exchange membrane channel and a pyrolyzer channel to determine Hg^{II} concentrations by difference. This system resulted in accurate Hg^{II} measurements at relatively rapid time intervals (10 min, though averaging over one or more hours improves detection limits) at our study site. Our design is based on the DOHGS instrument that has been used to measure Hg^{II} from aircraft,[11,49] but we have adapted it for long-term use at a surface measurement station. We provide information about this dual-channel system's performance and ambient air results. We base much of our assessment of its performance on verification with our automated mercury calibrator. We also present information about the calibrator's performance, including an attempt to verify the output of its permeation tubes gravimetrically.

2. MATERIALS AND METHODS

2.1. Sampling Location. We conducted the field component of this study at the Colorado Department of Public Health and Environment (CDPHE) air monitoring site at Rocky Flats National Wildlife Refuge in July and August 2018. The site is rural/suburban, and ∼25 km northwest of Denver, Colorado, U.S.A. (Figure S1 of the Supporting Information, SI). The station is located at latitude 39.913°, longitude −105.189°. Mercury point and area sources exist in the region (Figure S1), but the purpose of the field study was primarily to test the performance of a new dual-channel mercury measurement system, rather than to investigate nearby sources.

We measured Hg^0 and Hg^{II} with the dual-channel system, total atmospheric mercury with a separate analyzer, oxidized mercury with the UNR-RMAS 2.0 membrane sampling system,[28] and CO_2 with a LiCOR LI-840A at the field site. CDPHE measured the ozone and meteorological parameters. Details about measurement techniques appear below.

2.2. Mercury Calibration System. *2.2.1. Mercury Calibrator.* We used the same mercury calibrator that was described by Lyman et al.[43] The calibrator used permeation tubes to generate Hg^0, $HgBr_2$, and $HgCl_2$ vapor. The permeation tubes resided within deactivated fused silica-coated stainless steel tubing kept at constant temperature (nominally 100 °C) in a permeation oven. We describe the permeation tubes in the next section. High-purity nitrogen passed through the tubing and over the permeation tubes, and Hg^0 or Hg^{II} compounds emitted by the tubes traveled in the nitrogen stream to the calibrator outlet. A multiport valve allowed us to select among the available permeation tubes, and a LabView program allowed for automated, routine operation of the instrument. The calibrator maintained all tubing and valves downstream of the permeation tubes at 200 °C.

2.2.2. Permeation Tubes. We built permeation tubes that were similar to those described by Lyman et al.[43] The tubes were constructed of 3 mm PTFE or PFA tubing and had PTFE plugs at both ends to hold Hg^0, $HgBr_2$, and $HgCl_2$ in place within the tube. The permeable length (i.e., the distance between the plugs at the center of the tube) was approximately 1 mm. We constructed the permeation tubes used during the field deployment in Colorado from PFA tubing with 0.8 mm wall thickness, and we constructed the other permeation tubes used in this study from PTFE tubing with 0.2 mm wall thickness. For the Hg^0 permeation tube constructed of 0.2 mm tubing, we drilled a 1 mm diameter hole in one side of a PTFE rod, filled the hole with Hg^0, and covered the rod with the PTFE tubing. This limited the permeable area of the tube and kept the permeation rate low. We also constructed an empty permeation tube to determine the mass loss rate of the tube itself. (We constructed this tube like the others, but it contained no mercury.) We did not attempt injections from this blank permeation tube with the automated calibrator. We obtained Hg^0 from Sigma-Aldrich, and we purchased $HgBr_2$ and $HgCl_2$ from Sigma-Aldrich and American Elements.

We kept the permeation tubes either in the calibrator or in 40 mL amber glass vials with PTFE-lined caps. After construction, we only handled permeation tubes with PTFE-lined tweezers. When the calibrator was at the laboratory and the permeation tubes were housed within it (including the blank tube), we weighed the permeation tubes weekly with a Mettler Toledo XS3DU Microbalance to determine the rate of mercury loss. Gravimetric verification of mercury loss from diffusion tubes was first reported by Ent et al.[50] We used NIST-traceable mass standards to verify the performance of the balance on each day of use (acceptance criterion of ±4 μg). We passed permeation tubes through the poles of a Mettler Toledo 63052302 Haug Deionizer several times before each weighing to reduce errors from static electricity. We weighed permeation tubes repeatedly until the difference between two successive measurements was less than 3 μg, and we recorded the final mass. This usually required no more than three measurements. We calculated the Hg mass loss as the total mass loss multiplied by the fraction of the mass of the compounds in the permeation tubes that was due to Hg atoms (1.00 for Hg^0, 0.739 for $HgCl_2$, and 0.557 for $HgBr_2$). We excluded data from the first several weeks that a permeation tube was in the permeation oven, since the permeation tubes we constructed showed a rapid mass loss during this time, perhaps because of off-gasing from the Teflon material.

When the calibrator was in the laboratory, it was connected to a Tekran 1130 system and a Tekran 2537B mercury analyzer to determine the amount of Hg^0 and Hg^{II} injected by the calibrator. The Tekran 1130 collects Hg^{II} on KCl-coated quartz denuders. As discussed in the Introduction, KCl-coated

https://dx.doi.org/10.1021/acs.est.0c02747
Environ. Sci. Technol. 2020, 54, 13379−13388

denuders allow Hg^{II} compounds to decompose to Hg^0 when sampling ambient air, leading to a low bias. Available evidence suggests, however, that this bias does not occur if denuders sample air that has been purified by passing it through an activated carbon scrubber cartridge[42,44,51] (although KCl denuders do not appear to collect nonhalide mercury compounds quantitatively, even in scrubbed air).[37] We used the calibrator to inject Hg^0, $HgBr_2$, and $HgCl_2$ into the laboratory Tekran 1130 downstream of its elutriator/impactor inlet, since this inlet may collect oxidized mercury.[52]

The Hg^{II} permeation tubes emitted mercury at rates that led to unrealistically high mercury concentrations in sample air. To account for this, we injected for only a small portion of each measurement period (~10% of each measurement period for the 0.8 mm tubes and ~1% for the 0.2 mm tubes). This kept Hg^{II} recovered by the measurement systems within the range of hundreds of pg m^{-3}.

2.3. Dual-Channel Mercury Measurement System. We built a dual-channel mercury measurement system that operated similarly to the Detector of Oxidized Mercury (Hg) Species (DOHGS) used on airborne platforms (Figure 1).[11,49,53,54] Our dual-channel system pulled ambient air

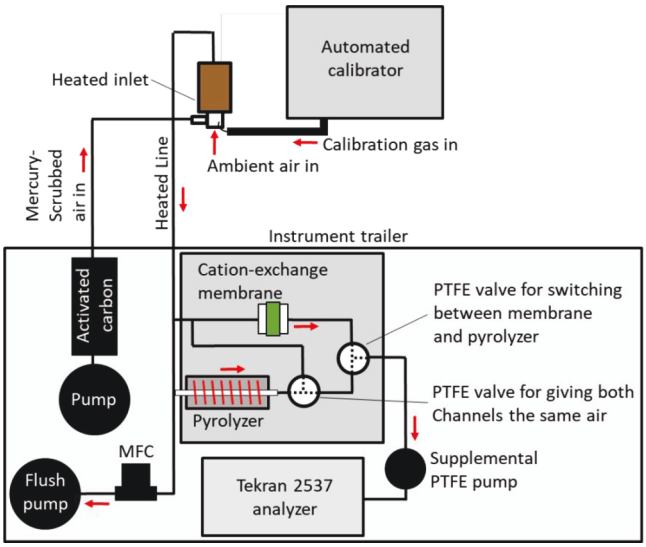

Figure 1. Diagram of the dual-channel measurement system.

through a PTFE-coated glass elutriator and particle impactor and then through a 6 mm PFA sample line at 10 L min^{-1} (volumetric) with a 50% particle cut size of 2.5 μm. URG corporation manufactured the elutriator and impactor. They were similar to the URG part numbers URG-2000-30K and URG-2000-30P that are components of the Tekran 1130 commercial mercury speciation system, except that they had a 6 mm stem added to the elutriator inlet. The system periodically forced excess purified air into this 6 mm stem to check for system contamination. The system maintained the inlet and sample line at 120 °C.

A Tekran 2537B mercury analyzer with a supplemental PTFE pump to maintain constant flow sequentially pulled 1 L min^{-1} from the sample line through (1) a series of two 47 mm-diameter cation-exchange membranes (housed in PFA filter holders) and (2) a pyrolyzer. The cation-exchange membranes collected oxidized mercury compounds while allowing Hg^0 to pass through.[55] The 650 °C pyrolyzer was a quartz tube filled with quartz wool, and had the same dimensions as the pyrolyzer described and tested by Lyman and Jaffe.[49] They showed that the pyrolyzer reduced at least 97% of $HgBr_2$ to Hg^0 (see their Supporting Information). A Campbell Scientific CR1000X datalogger controlled a PTFE valve that selected between the two channels.

The 2537 analyzer collected a gold trap sample every 2.5 min, and the datalogger sampled each channel for 5 min before switching to the next channel, so that one complete measurement occurred every 10 min (every four 2537 analyzer gold trap samples). The dual-channel valve switched at the same time as the 2537 analyzer gold traps). The CR1000X datalogger received the raw detector output from the 2537 analyzer at 0.1 s intervals. It (1) calculated the slope of the detector's baseline signal, (2) determined the time and magnitude of the maximum detector signal relative to the baseline slope (i.e., the maximum peak height relative to the baseline), and (3) calculated the mercury concentration by multiplying the maximum peak height by a calibration factor and dividing it by the analyzer's sample flow rate. The datalogger used the data output from the analyzer to update calibration factors for each of the analyzer's gold traps each time the analyzer performed an automated internal calibration.

The dual-channel system included a PTFE valve that allowed it to route air from downstream of the pyrolyzer to upstream of the cation-exchange membranes. Since air that had passed through the pyrolyzer contained only Hg^0, and since the membranes did not collect Hg^0,[55] activating this valve supplied both channels with the same Hg^{II}-free air. This allowed us to determine whether one channel was biased relative to the other. The datalogger activated this valve for two out of every 72 h, and we used these periods where both channels sampled the same air to calculate detection limits as three times the standard deviation of Hg^{II} measurements when the same-air valve was activated. The system also pumped air scrubbed of mercury via an activated carbon canister into the 6 mm stem on the system's inlet for two out of every 168 h.

We installed a soda lime trap, following AMNet methods,[56] upstream of the 2537 analyzer. We changed the soda lime every 2 weeks and changed the cation-exchange membranes weekly. The 2537 analyzer also performed automated internal permeation source calibrations every 71 h throughout the study.

We checked the calibration of the 2537 analyzer used for the dual-channel system and the total mercury (THg) system (see next section) with the automated calibrator, and by performing manual injections of Hg^0 vapor from a temperature-controlled mercury vapor source. We calculated the mercury vapor concentration in the source using the Dumarey equation.[57] Recovery of injected mercury vapor was 105 ± 6% for the dual-channel system.

The dual-channel ambient air data set is available via USU's Digital Commons Web site.[58]

2.4. Total Mercury Measurement System. We measured total atmospheric Hg (THg = Hg^0 + Hg^{II}) with an adjacent system to verify the dual-channel system's measurement capabilities. This system was housed in the same instrument shelter as the dual-channel system and sampled air from the same main sample line. For the THg system, a Tekran 2537A pulled air at 1 L min^{-1} from the main sample line through a pyrolyzer that was continuously heated to 650 °C to convert any Hg^{II} to Hg^0. The Tekran 2537A recorded 5 min integrated measurements that we later averaged to match the 10 min measurements from the dual-channel system. We

https://dx.doi.org/10.1021/acs.est.0c02747
Environ. Sci. Technol. 2020, 54, 13379−13388

analyzed the raw Tekran detector output to determine THg concentrations from peak height, as described by Swartzendruber et al.[59]

As with the dual-channel system, this system had a soda lime trap upstream of the 2537 analyzer, and we changed the soda lime every 2 weeks. The 2537 analyzer performed automated internal permeation source calibrations every 71 h throughout the study, and we performed manual injections of Hg^0 vapor from a temperature-controlled mercury vapor source (using the Dumarey equation[57]) to check instrument performance. Recovery of injected mercury vapor was 101 ± 1%.

2.5. Cation-Exchange Membrane Measurements with the UNR-RMAS 2.0. We used the UNR-RMAS 2.0 membrane sampling system to quantify Hg^{II} and determine Hg^{II} compounds at the field site from June through August 2018. Luippold et al.[28] recently described the operation of the UNR-RMAS in detail. Briefly, the UNR-RMAS pulls air at 1 L min^{-1} through 47 mm cation-exchange and nylon membranes housed in PFA filter holders. We sampled triplicate membranes of each membrane type over two-week periods. After sampling, we digested cation-exchange membranes in a BrCl solution and analyzed the digestate for THg concentration using cold vapor atomic fluorescence spectrometry. THg concentrations in the CEM digestates represent Hg^{II} since Hg^0 does not sorb to cation-exchange membranes.[55] We thermally desorbed nylon membranes following the procedures in Luippold et al.[33] to determine the oxidized mercury compounds present in the sampled air.

2.6. Other Measurements. CDPHE provided continuous 1 min ozone measurements from a Teledyne API T400 analyzer as well as 1 min measurements of temperature, wind speed, wind direction, and relative humidity. The CDPHE Quality Assurance Project Plan (QAPP)[60] contains the calibration and QA/QC procedures for these measurements. Hourly data generated by the CDPHE can be obtained through the U.S. EPA Air Quality System (AQS) database.[61] We also measured carbon dioxide with a LiCor LI-840A continuous CO_2/H_2O analyzer with an external pump that pulled air through 1/4 in. O.D., 1/8 in. I.D. Bev-A-Line polyethylene tubing. The inlet consisted of a Millipore-FA filter unit containing a 1.0 μm PTFE filter. Inlet heights for all chemical measurements were 4 m above ground and 1 m above the instrument shelter.

2.7. HYSPLIT. We used HYSPLIT to determine the origins of air masses that impacted the measurement station during the field campaign.[62] We computed 168-h back trajectories for 14:00 local standard time on each day between 8 and 17 August 2018, a period with both high and low daytime Hg^{II}. We used the GDAS 0.5° data set available on the HYSPLIT Web site.[63] HYSPLIT calculated vertical velocity from divergence. We used HYSPLIT's ensemble trajectory mode, in which the starting meteorological data points associated with trajectories (not the actual trajectory starting point) are offset in a 3-dimensional cube centered at the starting point. For this mode, the HYSPLIT software draws meteorological data from the corners, midpoints, and center of the cube, resulting in 27 meteorological data points. Our starting heights were approximately 150, 400, and 650 m (0.01 sigma units), and our horizontal spacing was about 10 km (about 0.1° latitude and longitude).

2.8. Data Processing and Analysis. Variability in internal calibration response led to differences between THg measured by the two 2537 analyzers. We applied a multiplier to dual-channel system data to minimize this discrepancy (multiplier = [THg system calibration response]/[dual-channel system calibration response]). The average difference between the systems over the study period was 12% (the dual-channel system was higher).

We analyzed the data from this study with IBM SPSS Statistics v22, Matlab vR2014b, and Microsoft Excel 2013. We calculated slopes using reduced major axis regression.[64] We used $\alpha = 0.05$ to determine statistical significance. We present results as average ±95% confidence interval unless otherwise indicated. We used 1-h average data for all statistical analyses.

3. RESULTS AND DISCUSSION

3.1. Permeation Tube Characterization. When kept heated in the calibrator's permeation oven, $HgBr_2$ and $HgCl_2$ permeation tubes constructed from PTFE tubing with 0.2 mm wall thickness lost mass a rate of 54.0 ± 1.4 and 42.1 ± 0.9 pg sec^{-1}, respectively, much higher than the tubes constructed with PFA tubing with 0.8 mm wall thickness (2.0 ± 0.5 and 4.1 ± 0.5 pg sec^{-1}, respectively). The Hg^0 permeation tube constructed of 0.2 mm thickness PTFE lost 3.6 ± 0.9 pg sec^{-1}, while the Hg^0 permeation tube constructed of 0.8 mm thickness PFA lost only 0.4 ± 0.6 pg sec^{-1} (the Hg^0 permeation tube constructed of 0.2 mm thickness PTFE had a smaller permeable area than similar permeation tubes filled with $HgBr_2$ and $HgCl_2$). The r^2 values of the mass loss slopes were related to (though not significantly correlated with) the magnitude of the mass loss rate, ranging from 1.00 for a loss rate of 53.9 pg sec^{-1} to 0.18 for a loss rate of 0.4 pg sec^{-1}. Figure 2 shows the mass loss for some of these permeation tubes. Figures S2–S4 and Table S1 provide additional information about mass loss from permeation tubes.

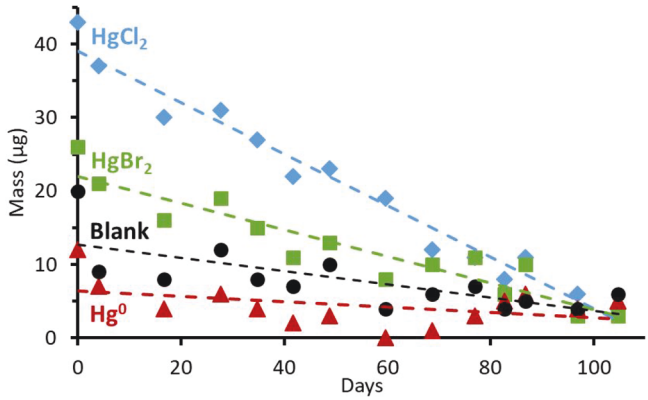

Figure 2. Change in mass over time for three permeation tubes ($HgBr_2$, $HgCl_2$, and Hg^0) constructed of PFA tubing with 0.8 mm wall thickness, and an empty (blank) permeation tube constructed of PTFE tubing with 0.2 mm wall thickness.

Figure 2 shows that the blank permeation tube lost mass at a higher rate (1.0 ± 0.1 pg sec^{-1}) than the Hg^0 permeation rate for the period shown. We began measuring the blank permeation tube's mass before the period shown in Figure 2 and continued measuring it after that period, for 675 days (measurement periods for permeation tubes that contained mercury were shorter). When calculated over this entire period, the mass loss rate of the blank permeation tube was only 0.1 ± 0.1 pg sec^{-1} (it was 0.3 ± 0.3 pg sec^{-1} for the period during which we measured the permeation tubes with 0.2 mm thickness tubing). It is not clear why the loss rate was higher

https://dx.doi.org/10.1021/acs.est.0c02747
Environ. Sci. Technol. 2020, 54, 13379−13388

for the period shown in Figure 2. We suspect that mass loss from the blank permeation tube was due to abrasion of the Teflon surface during handling and/or volatile loss of the tube's Teflon components.

Figure 3 shows the permeation rate of THg from the tubes constructed from 0.8 mm thickness PFA tubing, as determined

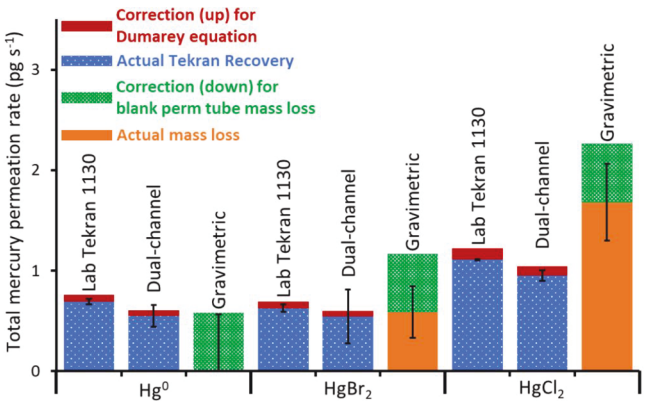

Figure 3. Emission rate of THg from three permeation tubes constructed from 0.8 mm PFA tubing. We determined emission rate by the loss of mass from the tubes over time and by the amount of Hg^0 + Hg^{II} recovered that was delivered by the calibrator to the field dual-channel system and the laboratory Tekran 2537/1130 system (the laboratory Tekran system sampled air scrubbed with an activated carbon cartridge). Whiskers show 95% confidence intervals. See the text for a discussion of the correction techniques applied.

from the rate of mass loss, and as recovered by the laboratory Tekran 2537/1130 system and the field dual-channel system. Figure S5 shows the same information for permeation tubes constructed from 0.2 mm thickness PTFE tubing. Because the blank permeation tube was constructed of PTFE, its mass loss rate may not have been representative of mass loss from the PFA permeation tubes (unfortunately, our study did not include a blank PFA permeation tube). Thus, the correction for blank permeation tube mass loss in Figure 3 has high uncertainty.

Evidence exists that the concentration of Hg^0 at saturation, as determined by the Dumarey equation,[57] is biased low.[50,65] We used the Dumarey equation to calculate Hg^0 concentrations in saturated mercury vapor injections conducted to calibrate all the Tekran 2537 analyzers. Direct, SI-traceable measurements by Quetel et al.[66] resulted in concentrations 10−12% higher than those determined by the Dumarey, and direct measurements by Srivastava et al.[67] were 8.5% higher. If this low bias in Dumarey-based Hg^0 calibrations is real, then it could account for some of the discrepancy between gravimetrically determined and analyzer-measured emission rates from permeation tubes. We included a 10% correction of the Tekran system measurements for this bias in Figures 3 and S5.

Also, as shown from our measurements with a blank permeation tube, mass loss occurs from the permeation tube materials, not just from loss of mercury, leading to a high bias in the mass loss measurements. We show a correction in Figures 3 and S5 for the mass loss that occurred from the blank permeation tube during the period that we wieghed each nonblank permeation tube.

Despite these corrections, the gravimetrically determined and analyzer-measured total mercury permeation rates did not always agree well. Gravimetrically determined $HgBr_2$ and $HgCl_2$ permeation rates for the 0.8 mm thickness tubes were 94 and 152%, respectively, of those determined by the laboratory Tekran system. Also, after correcting for mass loss from the blank permeation tube, the gravimetrically determined Hg^0 permeation rate was less than zero (although, as mentioned above, the blank tube was constructed differently from the PFA Hg^0 permeation tube, adding uncertainty to the blank correction). Permeation rates for the 0.2 mm thickness tubes were 120, 116, and 124% higher for Hg^0, $HgBr_2$, and $HgCl_2$, respectively, than those determined by the Tekran system, which was much more consistent than the 0.8 mm tubes. We expect this is because the 0.2 mm tubes emitted mercury at a much higher rate, so the mass loss rate had lower uncertainty, and any loss of nonmercury mass was insignificant (Figure S5).

The 0.2 mm tubes also emitted more mercury as Hg^{II} than the 0.8 mm permeation tubes. When used with the calibrator to inject into the laboratory Tekran 2537/1130 system that sampled air scrubbed with an activated carbon cartridge, 74 ± 2% of the mercury permeated by the tubes with 0.2 mm wall thickness was recovered as Hg^{II}. For the 0.8 mm thickness permeation tubes, 29 ± 2% was recovered as Hg^{II}. We do not yet know whether this difference was due to the thickness of the tubes or the tube material (0.2 mm tubes were PTFE, while 0.8 mm tubes were PFA).

The 0.2 mm PTFE tubes performed better than the 0.8 mm PFA tubes for the quality control results described here. The strong disadvantage of the 0.2 mm tubes, however, is that they lead to unrealistically high THg and Hg^{II} concentrations. Continuous injection from the 0.2 mm$HgBr_2$ tube into a 10 L min^{-1} stream of mercury-free air led to a THg concentration of 178 ng m^{-3}, while injection with the 0.8 mm$HgBr_2$ tube only led to an increase of 3.5 ng m^{-3}. As discussed in the Methods section, we kept measured concentrations low by injecting for only a portion of each measurement period (e.g., Hg^{II} injections were typically 10 or 20 s of the 150-s gold trap sampling time for the 0.8 mm tubes used in the dual-channel field study, resulting in THg enhancements of less than 500 pg m^{-3}). We acknowledge that this still leads to unrealistically high Hg^{II} concentrations during the short injection time and that this may have impacted our results.

3.2. Calibration Recovery. The permeation tubes with 0.2 mm wall thickness were the same as those used by Lyman et al.[43] When the calibrator and those permeation tubes were used with Tekran 2537/1130 systems sampling ambient air at field sites, they recovered a lower percentage of the emitted mercury as Hg^{II} than the Tekran 2537/1130 system that sampled scrubbed air in the laboratory (Figure 4). This is due to ambient air inhibiting the ability of the Tekran 2537/1130 systems to recover injected Hg^{II}.[39,43] In contrast, Figure 4 shows that the dual-channel measurement system and the laboratory Tekran 2537/1130 system that sampled scrubbed air collected a similar percentage of mercury injected from the permeation tubes as Hg^{II}. This provides evidence that the dual-channel system was able to collect Hg^{II} compounds quantitatively. Figure 3 shows that the two systems also recovered similar amounts of total mercury from all the permeation tubes.

We did not measure Hg^{II} with a KCl denuder-based system during our field deployment, and we cannot, therefore, be certain that such a system would have performed more poorly than our dual-channel system in that location and time of year. We submit, however, that all previous studies that have

https://dx.doi.org/10.1021/acs.est.0c02747
Environ. Sci. Technol. 2020, 54, 13379−13388

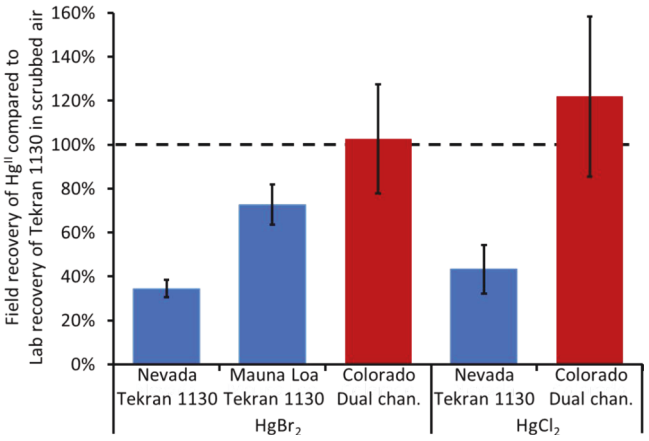

Figure 4. Comparison of Hg^{II} recovery by measurement systems in ambient air versus the laboratory Tekran 2537/1130 system that sampled air scrubbed with an activated carbon cartridge. Field measurements for the Tekran 1130 systems are from Lyman et al.[43] Each bar shows 100 × [fraction of injected mercury recovered as Hg^{II} by the field system indicated]/[fraction of injected mercury recovered as Hg^{II} by the laboratory Tekran 2537/1130 with the same permeation tubes]. Whiskers show 95% confidence intervals.

investigated the performance of KCl denuders have found that they are biased low in ambient air,[37,39,41−43,48,68] and that this short field study constitutes the first Hg^{II} measurements that have been shown with field calibrations to be quantitative. More work is needed to determine whether this dual-channel system can accurately measure Hg^{II} in a wide range of field conditions.

3.3. Dual-Channel Detection Limit. The Hg^{II} detection limit of the dual-channel system for each 10 min sample (calculated as three times the standard deviation of measurements when the system routed pyrolyzed air to the membrane channel) was 107 ± 23 pg m^{-3}. The 1-h detection limit (three times the standard deviation of 1-h averages) was 60 ± 34 pg m^{-3}. The 3-h detection limit was 33 pg m^{-3} (not enough data to calculated confidence interval).

Since almost all past Hg^{II} measurements have been based on biased KCl denuder systems, few reliable, and almost no calibrated, measurements of Hg^{II} are available to compare against the dual-channel system's detection limit. The detection limit was low enough to clearly distinguish diurnal patterns of Hg^{II} in this study (Figures 5 and S6), but it may be too high to be useful in places known to have relatively low atmospheric Hg^{II}, such as the eastern United States.[29]

3.4. Ambient Air Results. THg from the dual-channel and THg systems were reasonably well correlated (r^2 = 0.76; slope = 1.01 ± 0.04). Figure 5 shows a time series of THg from both systems and Hg^{II} from the dual-channel system and the UNR-RMAS. As Figure 5 shows, dual-channel Hg^{II} sometimes dropped below zero, but these deviations were rarely less than the 1-h detection limit.

Hg^{II} was correlated with ozone and temperature and anticorrelated with Hg^0, relative humidity, and CO_2 (Table S2), similar to what others have shown.[69−74] Correlations with Hg^0 showed opposite trends (statistically significant Pearson r values with ozone, humidity, and temperature were −0.33, 0.47, and −0.36, respectively). Hg^{II} tended to be higher during the day and lower at night, also consistent with other studies.[69,73] Figure S6 shows a diurnal plot of Hg^{II}, Hg^0, and ozone.

Hg^{II} tended to be highest when winds were from the east (Figure S7), and ozone displayed a similar directional pattern (data not shown). Easterly, upslope flow commonly occurs during the daytime along the Colorado Front Range.[75] To the southeast of the measurement station is the Denver metropolitan area (Figure S1), and to the direct east is an area of intensive oil and natural gas production. Both of these areas are abundant sources of ozone precursors.[76−78] The Colorado Front Range experiences local summertime photochemical ozone production,[78] and, given the correlation between ozone and Hg^{II}, it could be argued that Hg^{II} was also produced via local boundary layer photochemistry.[13,23]

Alternatively, the same high-pressure conditions that are conducive to local ozone photochemistry on the Front Range[79] are also conducive to transport of potentially Hg^{II}-rich free-tropospheric air to the surface.[11,80−82] Daily ensemble HYSPLIT back trajectories showed that afternoon Hg^{II} tended to be higher when trajectory paths were at higher average altitude (Pearson r = 0.83) and when average specific humidity was lower (r = 0.83). (Figures S8 and S9 show example trajectories from high- and low-Hg^{II} days, respectively.) The average altitude and specific humidity over the entire 168-h path for trajectories that ended on 11 August, a day with elevated afternoon Hg^{II} (Figure 5), were 8523 ± 128 m above sea level and 1.0 ± 0.1 g kg^{-1}, versus 3937 ± 102 m and 5.6 ± 0.1 g kg^{-1} on 8 August, a day with low afternoon Hg^{II}. Trajectories on low-Hg^{II} days also had more rainfall and less sunlight, though these trends were not statistically significant. This provides evidence that Hg^{II} measured at the study site may have originated from the dry free troposphere. While our field study was inadequate to distinguish between these two

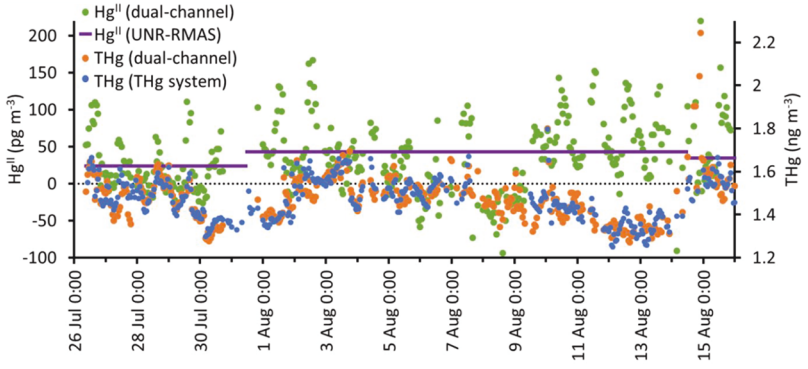

Figure 5. Time series of THg and Hg^{II} in ambient air. Hours are local standard time.

https://dx.doi.org/10.1021/acs.est.0c02747
Environ. Sci. Technol. 2020, 54, 13379−13388

possible sources (i.e., local photochemical production vs transport from the free troposphere), available evidence from other studies suggests that a free troposphere source may be more likely.[17,21,83]

Whole-campaign average Hg^{II} concentrations were higher than almost all KCl denuder measurements that have been made at ground-based monitoring stations, likely because KCl denuder measurements are biased low, while our measurement system appears to collect Hg^{II} quantitatively (Figure 4). Our study average was lower than summertime KCl denuder-based measurements at the Desert Research Institute near Reno, Nevada (51 ± 29 pg m^{-3}; mean ± standard deviation),[82] but was higher than summer measurements at other locations in Nevada (10−17 pg m^{-3}).[84] Our average was higher than late spring and summer measurements at Storm Peak Laboratory (20 ± 21 pg m^{-3}; mean ± standard deviation),[74] which lies at 3220 m above sea level (our study location is at 1650 m) and 150 km to the northwest of our study location. Our measurements were in the range of those collected at Mt. Bachelor, Oregon, another mountaintop site (39 pg m^{-3}),[81] and were much higher than previous measurements in the west-central U.S. (e.g., 7 ± 7 pg m^{-3} in New Mexico[85] and less than 7 pg m^{-3} in Oklahoma[86]).

Measurements of Hg^{II} using the UNR-RMAS system, in contrast, have shown higher concentrations than those measured by KCl denuder systems. Huang et al.[29] showed that cation-exchange membrane-derived Hg^{II} was more than ten times higher than KCl denuder-based measurements at a site in Florida, and Luippold et al.[28] found a difference of 3−10 times in Nevada.

The UNR-RMAS measurements in this study did not perfectly coincide with the short dual-channel sampling period, so a direct comparison of the two methods cannot be made. UNR-RMAS Hg^{II} averaged 35 ± 13 pg m^{-3} during July and August 2018, however, in the same range as our dual-channel measurements (also see Figure 5). As cation-exchange membrane-based measurements (and perhaps measurements from other new methods) proliferate, their apparently quantitative measurements of Hg^{II} will allow for a more accurate understanding of atmospheric mercury concentrations.[87,88] Consistent with previous studies,[28,29,37,68] Hg^{II} concentrations derived from nylon membrane samples were lower than those derived from cation-exchange membrane samples, although they exhibited similar temporal trends (Figure S10). On the basis of the nylon membrane thermal desorption profiles, Hg^{II} compounds containing halogens and nitrogen dominated during the sampling campaign (Figure S11), with halogen-containing compounds making up the majority of Hg^{II} during all sampling periods, and nitrogen-containing compounds present during the two-week sampling periods starting on July 3rd, July 17th, and August 14th. Evidence for sulfur-containing compounds existed during the August 14th sampling period. In previous work, halogen-containing Hg^{II} compounds tended to be associated with air from the upper atmosphere, while nitrogen- and sulfur-containing compounds were related to local anthropogenic pollution.[29,38] The dominance of halogen-containing compounds here adds strength to the hypothesis that most of the observed Hg^{II} originated in the upper troposphere.

3.5. Additional Work. Even though the dual-channel system was able to quantitatively detect $HgCl_2$ and $HgBr_2$ in ambient air, we are currently unable to verify its ability to quantitatively detect actual ambient Hg^{II}, since evidence indicates that ambient Hg^{II} is composed of multiple compounds.[6,28−31] The cation-exchange membranes used by the system have been shown to collect a diverse array of synthetic Hg^{II} compounds, and they perform much better than KCl denuders in this regard,[36−38] but additional work is needed to verify whether the membranes detect these compounds quantitatively in the dual channel system. Some Hg^{II} compounds that have been proposed (BrHgOOH, HgBrONO, and others[19,20,24,30−33,35]) have not been produced synthetically, rendering calibration for these specific compounds impossible, at least via permeation tube-based methods.

Our dual-channel measurement system shows promise, providing the first Hg^{II} measurements to date that have been demonstrated with field calibrations to be accurate. Its detection limit was relatively high, however, perhaps too high for meaningful measurements in some areas of the world. Since completion of the work reported here, we have decreased the 10 min and 1-h detection limits of the system to 38 ± 8 and 13 ± 2 pg m^{-3}, respectively, by improving the stability of the 2537 analyzer and the detector output processing method. We have also begun developing a version of the instrument in which we will minimize the potential for line loss of Hg^{II} by mounting the membrane and pyrolyzer channels on a sampling tower and reducing the inlet line length to ∼5 cm. Along with continuing research to better characterize permeation tubes and improve our automated calibrator, these advances will increase the precision and reliability of future Hg^{II} measurements.

■ ASSOCIATED CONTENT

Supporting Information

The Supporting Information is available free of charge at https://pubs.acs.org/doi/10.1021/acs.est.0c02747.

Hg^0 and Hg^{II} ambient air data set collected for this study is publicly available[58] (PDF)

■ AUTHOR INFORMATION

Corresponding Author

Seth N. Lyman − *Bingham Research Center and Department of Chemistry and Biochemistry, Utah State University, Vernal, Utah 84078, United States;* orcid.org/0000-0001-8493-9522; Email: seth.lyman@usu.edu

Authors

Lynne E. Gratz − *Environmental Studies Program, Colorado College, Colorado Springs, Colorado 80903-3298, United States;* orcid.org/0000-0002-7904-991X

Sarrah M. Dunham-Cheatham − *Department of Natural Resources and Environmental Science, University of Nevada—Reno, Reno, Nevada 89557, United States*

Mae Sexauer Gustin − *Department of Natural Resources and Environmental Science, University of Nevada—Reno, Reno, Nevada 89557, United States;* orcid.org/0000-0002-9306-2037

Adriel Luippold − *Department of Natural Resources and Environmental Science, University of Nevada—Reno, Reno, Nevada 89557, United States*

Complete contact information is available at: https://pubs.acs.org/10.1021/acs.est.0c02747

Notes

The authors declare no competing financial interest.

https://dx.doi.org/10.1021/acs.est.0c02747
Environ. Sci. Technol. 2020, 54, 13379−13388

■ ACKNOWLEDGMENTS

The U.S. National Science Foundation (grants 1700722, 1700711, and 1951513) and Colorado College (the Natural Sciences Division, the Southwest Studies Program Jackson Fellowship, the Student-Faculty Collaborative Research (SCoRe) program, Grant Lyddon, and the SEGway Program) funded this work. Dan Jaffe at the University of Washington loaned us most of the components that made up the dual-channel system. Erick Mattson at the Colorado Department of Public Health and Environment facilitated our measurement campaign at the Rocky Flats National Wildlife Refuge monitoring station. Darren Ceckanowicz of Colorado College assisted with site operation and data acquisition. Randy Anderson of Utah State University participated in construction, deployment, and operation of the dual-channel instrument. Colorado College Environmental Studies Program alumni Story Schwantes ('19) and Melissa Taing ('19) participated in data collection and preliminary analysis.

■ REFERENCES

(1) Zahir, F.; Rizwi, S. J.; Haq, S. K.; Khan, R. H. Low dose mercury toxicity and human health. *Environ. Toxicol. Pharmacol.* **2005**, *20* (2), 351−360.

(2) Houston, M. C. Role of mercury toxicity in hypertension, cardiovascular disease, and stroke. *J. Clin. Hypertens.* **2011**, *13* (8), 621−627.

(3) Mahbub, K. R.; Krishnan, K.; Naidu, R.; Andrews, S.; Megharaj, M. Mercury toxicity to terrestrial biota. *Ecol. Indic.* **2017**, *74*, 451−462.

(4) Weiss-Penzias, P. S.; Bank, M. S.; Clifford, D. L.; Torregrosa, A.; Zheng, B.; Lin, W.; Wilmers, C. C. Marine fog inputs appear to increase methylmercury bioaccumulation in a coastal terrestrial food web. *Sci. Rep.* **2019**, *9* (1), 1−11.

(5) Driscoll, C. T.; Mason, R. P.; Chan, H. M.; Jacob, D. J.; Pirrone, N. Mercury as a global pollutant: sources, pathways, and effects. *Environ. Sci. Technol.* **2013**, *47* (10), 4967−4983.

(6) Lin, C. J.; Pongprueksa, P.; Lindberg, S. E.; Pehkonen, S. O.; Byun, D.; Jang, C. Scientific uncertainties in atmospheric mercury models I: Model science evaluation. *Atmos. Environ.* **2006**, *40* (16), 2911−2928.

(7) Obrist, D.; Kirk, J. L.; Zhang, L.; Sunderland, E. M.; Jiskra, M.; Selin, N. E. A review of global environmental mercury processes in response to human and natural perturbations: Changes of emissions, climate, and land use. *Ambio* **2018**, *47* (2), 116−140.

(8) Muntean, M.; Janssens-Maenhout, G.; Song, S.; Giang, A.; Selin, N. E.; Zhong, H.; Zhao, Y.; Olivier, J. G.; Guizzardi, D.; Crippa, M.; Schaaf, E.; Dentener, F. Evaluating EDGARv4. tox2 speciated mercury emissions ex-post scenarios and their impacts on modelled global and regional wet deposition patterns. *Atmos. Environ.* **2018**, *184*, 56−68.

(9) Sprovieri, F.; Pirrone, N.; Bencardino, M.; D'Amore, F.; Carbone, F.; Cinnirella, S.; Mannarino, V.; Landis, M.; Ebinghaus, R.; Weigelt, A.; et al. Atmospheric Mercury Concentrations observed at ground-based monitoring sites globally distributed in the framework of the GMOS network. *Atmos. Chem. Phys.* **2016**, *16* (18), 11915−11935.

(10) Coburn, S.; Dix, B.; Edgerton, E.; Holmes, C. D.; Kinnison, D.; Liang, Q.; ter Schure, A.; Wang, S.; Volkamer, R. Mercury oxidation from bromine chemistry in the free troposphere over the southeastern US. *Atmos. Chem. Phys.* **2016**, *16* (6), 3743−3760.

(11) Gratz, L.; Ambrose, J.; Jaffe, D.; Shah, V.; Jaeglé, L.; Stutz, J.; Festa, J.; Spolaor, M.; Tsai, C.; Selin, N.; et al. Oxidation of mercury by bromine in the subtropical Pacific free troposphere. *Geophys. Res. Lett.* **2015**, *42* (23), 10494−10502.

(12) Holmes, C. D.; Jacob, D. J.; Corbitt, E. S.; Mao, J.; Yang, X.; Talbot, R.; Slemr, F. Global atmospheric model for mercury including oxidation by bromine atoms. *Atmos. Chem. Phys.* **2010**, *10* (24), 12037−12057.

(13) Ye, Z.; Mao, H.; Lin, C.-J.; Kim, S. Y. Investigation of processes controlling summertime gaseous elemental mercury oxidation at midlatitudinal marine, coastal, and inland sites. *Atmos. Chem. Phys.* **2016**, *16* (13), 8461−8478.

(14) Peleg, M.; Tas, E.; Matveev, V.; Obrist, D.; Moore, C. W.; Gabay, M.; Luria, M. Observational evidence for involvement of nitrate radicals in nighttime oxidation of mercury. *Environ. Sci. Technol.* **2015**, *49* (24), 14008−14018.

(15) Tong, Y.; Eichhorst, T.; Olson, M. R.; McGinnis, J. E.; Turner, I.; Rutter, A. P.; Shafer, M. M.; Wang, X.; Schauer, J. J. Atmospheric photolytic reduction of Hg (II) in dry aerosols. *Environ. Sci. Proc. Imp.* **2013**, *15* (10), 1883−1888.

(16) Zubatiuk, T.; Hill, G.; Leszczynski, J. How water affects mercury−halogen interaction in the atmosphere. *J. Mol. Model.* **2019**, *25* (12), 357.

(17) Lyman, S. N.; Cheng, I.; Gratz, L. E.; Weiss-Penzias, P.; Zhang, L. An updated review of atmospheric mercury. *Sci. Total Environ.* **2020**, *707*, 135575.

(18) Gustin, M.; Dunham-Cheatham, S. M.; Zhang, L. Comparison of four methods for measurement of reactive, gaseous oxidized, and particulate bound mercury. *Environ. Sci. Technol.* **2019**, *53*, 14489−14495.

(19) Horowitz, H. M.; Jacob, D. J.; Zhang, Y.; Dibble, T. S.; Slemr, F.; Amos, H. M.; Schmidt, J. A.; Corbitt, E. S.; Marais, E. A.; Sunderland, E. M. A new mechanism for atmospheric mercury redox chemistry: Implications for the global mercury budget. *Atmos. Chem. Phys.* **2017**, *17* (10), 6353−6371.

(20) Jiao, Y.; Dibble, T. S. First kinetic study of the atmospherically important reactions BrHg+ NO 2 and BrHg+ HOO. *Phys. Chem. Chem. Phys.* **2017**, *19* (3), 1826−1838.

(21) Saiz-Lopez, A.; Sitkiewicz, S. P.; Roca-Sanjuán, D.; Oliva-Enrich, J. M.; Dávalos, J. Z.; Notario, R.; Jiskra, M.; Xu, Y.; Wang, F.; Thackray, C. P.; et al. Photoreduction of gaseous oxidized mercury changes global atmospheric mercury speciation, transport and deposition. *Nat. Commun.* **2018**, *9* (1), 4796.

(22) Weiss-Penzias, P.; Amos, H.; Selin, N.; Gustin, M.; Jaffe, D.; Obrist, D.; Sheu, G.-R.; Giang, A. Use of a global model to understand speciated atmospheric mercury observations at five high-elevation sites. *Atmos. Chem. Phys.* **2015**, *15* (3), 1161−1173.

(23) Travnikov, O.; Angot, H.; Artaxo, P.; Bencardino, M.; Bieser, J.; D'Amore, F.; Dastoor, A.; De Simone, F.; DIéguez, M. C.; Dommergue, A.; Ebinghaus, R.; Feng, X. B.; Gencarelli, C. N.; Hedgecock, I. M.; Magand, O.; Martin, L.; Matthias, V.; Mashyanov, N.; Pirrone, N.; Ramachandran, R.; Read, K. A.; Ryjkov, A.; Selin, N. E.; Sena, F.; Song, S.; Sprovieri, F.; Wip, D.; Wangberg, I.; Yang, X. Multi-model study of mercury dispersion in the atmosphere: atmospheric processes and model evaluation. *Atmos. Chem. Phys.* **2017**, *17*, 5271−5295.

(24) Dibble, T. S.; Tetu, H. L.; Jiao, Y.; Thackray, C. P.; Jacob, D. J. Modeling the OH-Initiated Oxidation of Mercury in the Global Atmosphere Without Violating Physical Laws. *J. Phys. Chem. A* **2020**, *124* (2), 444−453.

(25) Khalizov, A. F.; Guzman, F. J.; Cooper, M.; Mao, N.; Antley, J.; Bozzelli, J. Direct detection of gas-phase mercuric chloride by ion drift-Chemical ionization mass spectrometry. *Atmos. Environ.* **2020**, *238*, 117687.

(26) Jones, C. P.; Lyman, S. N.; Jaffe, D. A.; Allen, T.; O'Neil, T. L. Detection and quantification of gas-phase oxidized mercury compounds by GC/MS. *Atmos. Meas. Tech.* **2016**, *9* (5), 2195−2205.

(27) Deeds, D. A.; Ghoshdastidar, A.; Raofie, F.; Guérette, E. l.-A. e.; Tessier, A.; Ariya, P. A. Development of a Particle-Trap Preconcentration-Soft Ionization Mass Spectrometric Technique for the Quantification of Mercury Halides in Air. *Anal. Chem.* **2015**, *87*, 5109−5116.

(28) Luippold, A.; Gustin, M. S.; Dunham-Cheatham, S. M.; Zhang, L. Improvement of quantification and identification of atmospheric reactive mercury. *Atmos. Environ.* **2020**, *224*, 117307.

(29) Huang, J.; Miller, M. B.; Edgerton, E.; Sexauer Gustin, M. Deciphering potential chemical compounds of gaseous oxidized mercury in Florida, USA. *Atmos. Chem. Phys.* **2017**, *17* (3), 1689−1698.
(30) Saiz-Lopez, A.; Acuña, A. U.; Trabelsi, T.; Carmona-García, J.; Dávalos, J. Z.; Rivero, D.; Cuevas, C. A.; Kinnison, D. E.; Sitkiewicz, S. P.; Roca-Sanjuán, D.; Francisco, J. Gas-Phase Photolysis of Hg (I) Radical Species: A New Atmospheric Mercury Reduction Process. *J. Am. Chem. Soc.* **2019**, *141*, 8698−8702.
(31) Sitkiewicz, S. P.; Rivero, D.; Oliva-Enrich, J. M.; Saiz-Lopez, A.; Roca-Sanjuán, D. Ab initio quantum-chemical computations of the absorption cross sections of HgX 2 and HgXY (X, Y= Cl, Br, and I): molecules of interest in the Earth's atmosphere. *Phys. Chem. Chem. Phys.* **2019**, *21* (1), 455−467.
(32) Dibble, T.; Zelie, M.; Mao, H. Thermodynamics of reactions of ClHg and BrHg radicals with atmospherically abundant free radicals. *Atmos. Chem. Phys.* **2012**, *12* (21), 10271−10279.
(33) Dibble, T. S.; Schwid, A. C. Thermodynamics limits the reactivity of BrHg radical with volatile organic compounds. *Chem. Phys. Lett.* **2016**, *659*, 289−294.
(34) Jiao, Y.; Dibble, T. S. Structures, Vibrational Frequencies, and Bond Energies of the BrHgOX and BrHgXO Species Formed in Atmospheric Mercury Depletion Events. *J. Phys. Chem. A* **2017**, *121* (41), 7976−7985.
(35) Lam, K. T.; Wilhelmsen, C. J.; Schwid, A. C.; Jiao, Y.; Dibble, T. S. Computational Study on the Photolysis of BrHgONO and the Reactions of BrHgO● with CH4, C2H6, NO, and NO2: Implications for Formation of Hg (II) Compounds in the Atmosphere. *J. Phys. Chem. A* **2019**, *123*, 1637−1647.
(36) Huang, J.; Gustin, M. S. Uncertainties of Gaseous Oxidized Mercury Measurements Using KCl-Coated Denuders, Cation-Exchange Membranes, and Nylon Membranes: Humidity Influences. *Environ. Sci. Technol.* **2015**, *49* (10), 6102−6108.
(37) Huang, J.; Miller, M. B.; Weiss-Penzias, P.; Gustin, M. S. Comparison of gaseous oxidized Hg measured by KCl-coated denuders, and nylon and cation exchange membranes. *Environ. Sci. Technol.* **2013**, *47* (13), 7307−7316.
(38) Gustin, M. S.; Pierce, A. M.; Huang, J.; Miller, M. B.; Holmes, H.; Loria-Salazar, S. M. Evidence for different reactive Hg sources and chemical compounds at adjacent valley and high elevation locations. *Environ. Sci. Technol.* **2016**, *50* (22), 12225−12231.
(39) McClure, C. D.; Jaffe, D. A.; Edgerton, E. S. Evaluation of the KCl denuder method for gaseous oxidized mercury using HgBr2 at an in-service AMNet site. *Environ. Sci. Technol.* **2014**, *48* (19), 11437−11444.
(40) Gustin, M. S.; Amos, H. M.; Huang, J.; Miller, M. B.; Heidecorn, K. Measuring and modeling mercury in the atmosphere: a critical review. *Atmos. Chem. Phys.* **2015**, *15* (10), 5697−5713.
(41) Bu, X.; Zhang, H.; Lv, G.; Lin, H.; Chen, L.; Yin, X.; Shen, G.; Yuan, W.; Zhang, W.; Wang, X.; Tong, Y. Comparison of Reactive Gaseous Mercury Collection by Different Sampling Methods in a Laboratory Test and Field Monitoring. *Environ. Sci. Technol. Lett.* **2018**, *5* (10), 600−607.
(42) Lyman, S. N.; Jaffe, D. A.; Gustin, M. S. Release of mercury halides from KCl denuders in the presence of ozone. *Atmos. Chem. Phys.* **2010**, *10* (17), 8197−8204.
(43) Lyman, S.; Jones, C.; O'Neil, T.; Allen, T.; Miller, M.; Gustin, M. S.; Pierce, A. M.; Luke, W.; Ren, X.; Kelley, P. Automated Calibration of Atmospheric Oxidized Mercury Measurements. *Environ. Sci. Technol.* **2016**, *50* (23), 12921−12927.
(44) Feng, X. B.; Sommar, J.; Gardfeldt, K.; Lindqvist, O. Improved determination of gaseous divalent mercury in ambient air using KCl coated denuders. *Fresenius' J. Anal. Chem.* **2000**, *366* (5), 423−428.
(45) Jaffe, D. A.; Lyman, S.; Amos, H. M.; Gustin, M. S.; Huang, J.; Selin, N. E.; Levin, L.; Ter Schure, A.; Mason, R. P.; Talbot, R.; Rutter, A.; Finley, B.; Jaeglé, L.; Shah, V.; McClure, C. D.; Ambrose, J. L.; Gratz, L.; Lindberg, S.; Weiss-Penzias, P.; Sheu, G. R.; Feddersen, D.; Horvat, M.; Dastoor, A.; Hynes, A.; Mao, H.; Sonke, J. E.; Slemr, F.; Fisher, J. A.; Ebinghaus, R.; Zhang, Y.; Edwards, G. Progress on understanding atmospheric mercury hampered by uncertain measurements. *Environ. Sci. Environ. Sci. Technol.* **2014**, *48* (13), 7204−7206.
(46) Finley, B. D.; Jaffe, D. A.; Call, K.; Lyman, S.; Gustin, M. S.; Peterson, C.; Miller, M.; Lyman, T. Development, testing, and deployment of an air sampling manifold for spiking elemental and oxidized mercury during the Reno Atmospheric Mercury Intercomparison Experiment (RAMIX). *Environ. Sci. Technol.* **2013**, *47* (13), 7277−7284.
(47) Sari, S.; Timo, R.; Jussi, H.; Panu, H. Dynamic calibration method for reactive gases. *Meas. Sci. Technol.* **2020**, *31* (3), No. 034001.
(48) Gustin, M. S.; Huang, J.; Miller, M. B.; Peterson, C.; Jaffe, D. A.; Ambrose, J.; Finley, B. D.; Lyman, S. N.; Call, K.; Talbot, R.; Feddersen, D.; Mao, H.; Lindberg, S. Do we understand what the mercury speciation instruments are actually measuring? Results of RAMIX. *Environ. Sci. Technol.* **2013**, *47* (13), 7295−7306.
(49) Lyman, S. N.; Jaffe, D. A. Elemental and oxidized mercury in the upper troposphere and lower stratosphere. *Nat. Geosci.* **2012**, *5*, 114−117.
(50) Ent, H.; van Andel, I.; Heemskerk, M.; van Otterloo, P.; Bavius, W.; Baldan, A.; Horvat, M.; Brown, R. J.; Quétel, C. R. A gravimetric approach to providing SI traceability for concentration measurement results of mercury vapor at ambient air levels. *Meas. Sci. Technol.* **2014**, *25* (11), 115801.
(51) Landis, M. S.; Stevens, R. K.; Schaedlich, F.; Prestbo, E. M. Development and characterization of an annular denuder methodology for the measurement of divalent inorganic reactive gaseous mercury in ambient air. *Environ. Sci. Technol.* **2002**, *36* (13), 3000−3009.
(52) Feng, X.; Lu, J. Y.; Hao, Y.; Banic, C.; Schroeder, W. H. Evaluation and applications of a gaseous mercuric chloride source. *Anal. Bioanal. Chem.* **2003**, *376* (7), 1137−1140.
(53) Gratz, L.; Ambrose, J.; Jaffe, D.; Knote, C.; Jaeglé, L.; Selin, N.; Campos, T.; Flocke, F.; Reeves, M.; Stechman, D.; Stell, M.; Weinheimer, A.; Knapp, D. J.; Montzka, D. D.; Tyndall, G.; Mauldin, R. L.; Cantrell, C. A.; Apel, E. C.; Hornbrook, R. S.; Blake, N. Airborne observations of mercury emissions from the Chicago/Gary urban/industrial area during the 2013 NOMADSS campaign. *Atmos. Atmos. Environ.* **2016**, *145*, 415−423.
(54) Ambrose, J. L.; Gratz, L. E.; Jaffe, D. A.; Campos, T.; Flocke, F. M.; Knapp, D. J.; Stechman, D. M.; Stell, M.; Weinheimer, A. J.; Cantrell, C. A.; Mauldin, R. L. Mercury emission ratios from coal-fired power plants in the Southeastern United States during NOMADSS. *Environ. Sci. Technol.* **2015**, *49* (17), 10389−10397.
(55) Miller, M. B.; Dunham-Cheatham, S. M.; Gustin, M. S.; Edwards, G. C. Evaluation of cation exchange membrane performance under exposure to high Hg0 and HgBr2 concentrations. *Atmos. Meas. Tech.* **2019**, *12* (2), 1207−1217.
(56) Gay, D. A.; Schmeltz, D.; Prestbo, E.; Olson, M.; Sharac, T.; Tordon, R. The Atmospheric Mercury Network: measurement and initial examination of an ongoing atmospheric mercury record across North America. *Atmos. Chem. Phys.* **2013**, *13* (22), 11339−11349.
(57) Dumarey, R.; Brown, R. J.; Corns, W. T.; Brown, A. S.; Stockwell, P. B. Elemental mercury vapour in air: the origins and validation of the 'Dumarey equation'describing the mass concentration at saturation. *Accredit. Qual. Assur.* **2010**, *15* (7), 409−414.
(58) Lyman, S. N.; Gratz, L. E. *Elemental and Oxidized Mercury in Ambient Air at Rocky Flats, Colorado*; Utah State University: Logan, UT, 2019, https://digitalcommons.usu.edu/all_datasets/73.
(59) Swartzendruber, P.; Jaffe, D.; Finley, B. Development and first results of an aircraft-based, high time resolution technique for gaseous elemental and reactive (oxidized) gaseous mercury. *Environ. Sci. Technol.* **2009**, *43* (19), 7484−7489.
(60) CDPHE. *Air Pollution Control Division Technical Services Program Quality Assurance Project Plan*; Colorado Department of Public Health and Environment: Denver, CO, 2015, https://www.colorado.gov/airquality/tech_doc_repository.aspx?action=open&file=APCD_QAPP_07302015.pdf.

https://dx.doi.org/10.1021/acs.est.0c02747
Environ. Sci. Technol. 2020, 54, 13379−13388

(61) U. S. EPA. U. S. EPA AQS Database, http://www.epa.gov/ttn/airs/airsaqs/ (accessed 3/10/2020).
(62) Draxler, R. R.; Rolph, G. D. *HYSPLIT (HYbrid Single-Particle Lagrangian Integrated Trajectory) modelNOAA Air Resources Laboratory*; NOAA Air Resources Laboratory: Silver Spring, MD, 2003.
(63) NOAA. *NOAA GDAS 0.5 Degree Dataset Description*; National Oceanic and Atmospheric Administration Air Resources Laboratory: College Park, MD, 2017, https://www.ready.noaa.gov/data/archives/gdas0p5/readme_gdas0p5_info.txt.
(64) Bohonak, A. J. *RMA: Software for Reduced Major Axis regression*; http://www.bio.sdsu.edu/pub/andy/RMA.html.
(65) Quétel, C. R.; Zampella, M.; Brown, R. J.; Ent, H.; Horvat, M.; Paredes, E.; Tunc, M. International system of units traceable results of Hg mass concentration at saturation in air from a newly developed measurement procedure. *Anal. Chem.* **2014**, *86* (15), 7819−7827.
(66) Quétel, C. R.; Zampella, M.; Brown, R. J. C. Temperature dependence of Hg vapour mass concentration at saturation in air: New SI traceable results between 15 and 30°C. *TrAC, Trends Anal. Chem.* **2016**, *85*, 81−88.
(67) Srivastava, A.; Hodges, J. T. Development of a High-Resolution Laser Absorption Spectroscopy Method with Application to the Determination of Absolute Concentration of Gaseous Elemental Mercury in Air. *Anal. Chem.* **2018**, *90* (11), 6781−6788.
(68) Huang, J.; Miller, M. B.; Edgerton, E.; Gustin, M. S. Use of criteria pollutants, active and passive mercury sampling, and receptor modeling to understand the chemical forms of gaseous oxidized mercury in Florida. *Atmos. Chem. Phys. Discuss.* **2015**, *15* (8), 12069−12105.
(69) Choi, H.-D.; Huang, J.; Mondal, S.; Holsen, T. M. Variation in concentrations of three mercury (Hg) forms at a rural and a suburban site in New York State. *Sci. Total Environ.* **2013**, *448*, 96−106.
(70) Weiss-Penzias, P. S.; Gustin, M. S.; Lyman, S. N. Sources of gaseous oxidized mercury and mercury dry deposition at two southeastern US sites. *Atmos. Environ.* **2011**, *45* (27), 4569−4579.
(71) Lyman, S. N.; Gustin, M. S. Determinants of atmospheric mercury concentrations in Reno, Nevada. *Sci. Total Environ.* **2009**, *408*, 431−438.
(72) Cheng, I.; Zhang, L.; Mao, H.; Blanchard, P.; Tordon, R.; Dalziel, J. Seasonal and diurnal patterns of speciated atmospheric mercury at a coastal-rural and a coastal-urban site. *Atmos. Environ.* **2014**, *82*, 193−205.
(73) Han, Y.-J.; Kim, J.-E.; Kim, P.-R.; Kim, W.-J.; Yi, S.-M.; Seo, Y.-S.; Kim, S.-H. General trends of atmospheric mercury concentrations in urban and rural areas in Korea and characteristics of high-concentration events. *Atmos. Environ.* **2014**, *94*, 754−764.
(74) Fain, X.; Obrist, D.; Hallar, A. G.; McCubbin, I.; Rahn, T. High levels of reactive gaseous mercury observed at a high elevation research laboratory in the Rocky Mountains. *Atmos. Chem. Phys.* **2009**, *9* (20), 8049−8060.
(75) Baumann, K.; Williams, E. J.; Olson, J. A.; Harder, J. W.; Fehsenfeld, F. C. Meteorological characteristics and spatial extent of upslope events during the 1993 Tropospheric OH Photochemistry Experiment. *J. Geophys. Res. Atmos.* **1997**, *102* (D5), 6199−6213.
(76) McDuffie, E. E.; Edwards, P. M.; Gilman, J. B.; Lerner, B. M.; Dubé, W. P.; Trainer, M.; Wolfe, D. E.; Angevine, W. M.; deGouw, J.; Williams, E. J.; Tevlin, A. G.; Murphy, J. G.; Fischer, E. V.; McKeen, S.; Ryerson, T.; Peischl, J.; Holloway, J.; Aikin, K.; Langford, A.; Senff, C.; Alvarez, R. J.; Hall, S.; Ullmann, K.; Lantz, K. O.; Brown, S. S. Influence of oil and gas emissions on summertime ozone in the Colorado Northern Front Range. *J. Geophys. Res. Atmos.* **2016**, *121* (14), 8712−8729.
(77) Evans, J. M.; Helmig, D. Investigation of the influence of transport from oil and natural gas regions on elevated ozone levels in the northern Colorado front range. *J. Air Waste Manage. Assoc.* **2017**, *67* (2), 196−211.
(78) Oltmans, S.; Cheadle, L.; Johnson, B.; Schnell, R.; Helmig, D.; Thompson, A.; Cullis, P.; Hall, E.; Jordan, A.; Sterling, C.; McClure-Begley, A.; Sullivan, J. T.; McGee, T. J.; Wolfe, D. Boundary layer ozone in the Northern Colorado Front Range in July−August 2014 during FRAPPE and DISCOVER-AQ from vertical profile measurements. *Elem. Sci. Anth.* **2019**, *7* (1), 6.
(79) Sullivan, J. T.; McGee, T. J.; Langford, A. O.; Alvarez, R. J.; Senff, C. J.; Reddy, P. J.; Thompson, A. M.; Twigg, L. W.; Sumnicht, G. K.; Lee, P.; et al. Quantifying the contribution of thermally driven recirculation to a high-ozone event along the Colorado Front Range using lidar. *J. Geophys. Res. Atmos.* **2016**, *121* (17), 10377−10390.
(80) Weiss-Penzias, P.; Gustin, M. S.; Lyman, S. N. Observations of speciated atmospheric mercury at three sites in Nevada: Evidence for a free tropospheric source of reactive gaseous mercury. *J. Geophys. Res.* **2009**, *114*, D14.
(81) Swartzendruber, P. C.; Jaffe, D. A.; Prestbo, E. M.; Weiss-Penzias, P.; Selin, N. E.; Park, R.; Jacob, D. J.; Strode, S.; Jaeglé, L. Observations of reactive gaseous mercury in the free troposphere at the Mt. Bachelor Observatory. *J. Geophys. Res.* **2006**, *111*, D24301.
(82) Peterson, C.; Gustin, M.; Lyman, S. Atmospheric mercury concentrations and speciation measured from 2004 to 2007 in Reno, Nevada, USA. *Atmos. Environ.* **2009**, *43* (30), 4646−4654.
(83) Hynes, A. J.; Donohoue, D. L.; Goodsite, M. E.; Hedgecock, I. M. Our current understanding of major chemical and physical processes affecting mercury dynamics in the atmosphere and at the air−water/terrestrial interfaces. In *Mercury Fate and Transport in the Global Atmosphere*; Mason, R., Pirrone, N., Eds.; Springer: New York, 2009; pp 427−457.
(84) Lyman, S. N.; Gustin, M. S. Speciation of atmospheric mercury at two sites in northern Nevada, USA. *Atmos. Environ.* **2008**, *42* (5), 927−939.
(85) Caldwell, C. A.; Swartzendruber, P.; Prestbo, E. Concentration and Dry Deposition of Mercury Species in Arid South Central New Mexico (2001−2002). *Environ. Sci. Technol.* **2006**, *40*, 7535.
(86) Sather, M. E.; Mukerjee, S.; Smith, L.; Mathew, J.; Jackson, C.; Callison, R.; Scrapper, L.; Hathcoat, A.; Adam, J.; Keese, D.; et al. Gaseous oxidized mercury dry deposition measurements in the Four Corners area and Eastern Oklahoma, USA. *Atmos. Pollut. Res.* **2013**, *4* (2), 168−180.
(87) Cheng, I.; Zhang, L. Uncertainty assessment of gaseous oxidized mercury measurements collected by Atmospheric Mercury Network. *Environ. Sci. Technol.* **2017**, *51* (2), 855−862.
(88) Shah, V.; Jaeglé, L.; Gratz, L.; Ambrose, J.; Jaffe, D.; Selin, N.; Song, S.; Campos, T.; Flocke, F.; Reeves, M.; et al. Origin of oxidized mercury in the summertime free troposphere over the southeastern US. *Atmos. Chem. Phys.* **2016**, *16* (3), 1511−1530.

https://dx.doi.org/10.1021/acs.est.0c02747
Environ. Sci. Technol. 2020, 54, 13379−13388